Journal of Molecular Liquids 346 (2022) 117047

Contents lists available at ScienceDirect

Journal of Molecular Liquids

journal homepage: www.elsevier.com/locate/molliq

Formation of mono- and binuclear complexes of Nd^{3+} with D-gluconate ions in hyperalkaline solutions – Composition, equilibria and structure

Éva Böszörményi [a,b], Zsolt Kása [a,b], Gábor Varga [b,c], Zoltán Kele [d], Bence Kutus [a,b,e], Gábor Peintler [b,f], István Pálinkó [b,c,†], Pál Sipos [a,b,*]

[a] Department of Inorganic and Analytical Chemistry, University of Szeged, Dóm tér 7, H-6720 Szeged, Hungary
[b] Material and Solution Structure Research Group, Institute of Chemistry, University of Szeged, Aradi Vértanúk tere 1, Szeged H-6720, Hungary
[c] Department of Organic Chemistry, University of Szeged, Dóm tér 8, H-6720 Szeged, Hungary
[d] Department of Medical Chemistry,University of Szeged, H–6720 Szeged, Dóm Sqr. 8, Hungary
[e] Max Planck Institute for Polymer Research, D-55128 Mainz, Ackermannweg 10
[f] Department of Physical Chemistry and Material Science, University of Szeged, Rerrich Béla Sqr. 1, H-6720 Szeged, Hungary

ARTICLE INFO

Article history:
Received 9 May 2021
Revised 15 July 2021
Accepted 17 July 2021
Available online 23 July 2021

Keywords:
D-Gluconate
Nd^{3+}
Potentiometry
Vis-spectrophotometry
Complex formation
Solution equilibria
L/ILW repositories

ABSTRACT

The composition and stability constants (or formation constants) of complexes comprising of D-gluconate ($Gluc^-$) and Nd^{3+} has been determined *via* potentiometry and Vis-spectrophotometry in aqueous solutions at 4.0 M (NaCl) ionic strength and in alkaline conditions. The chemical model derived from these measurements were complemented with freezing-point depression, Raman, ESI-MS and $^1H/^{13}C$ NMR measurements, some of these contributed to reveal structural features of the complexes formed. The presence of four variously protonated binuclear ($Nd_2Gluc_4H_{-5}^{3-}$, $Nd_2Gluc_4H_{-6}^{4-}$, $Nd_2Gluc_6H_{-4}^{4-}$, $Nd_2Gluc_6H_{-5}^{5-}$) and a mononuclear ($NdGluc_2H_{-5}^{4-}$) complexes were detected in highly alkaline media. The main coordination sites are the carboxylate and the alcoholate group attached to the C2 and C3 carbon atoms. The chemical picture obtained from our studies is of potential relevance in modeling some aspects of the aqueous chemistry of low or intermediate level radioactive waste (L/ILW) repositories.

1. Introduction

Possible complexing processes in L/ILW radioactive waste repositories have been excessively studied in the past decades. The radionuclide retention properties of concrete are an essential factor [1], which can be affected by complexing agents present, such as D-gluconate ($Gluc^-$), which is added to cement to improve certain properties such as delaying cement settling [2] or improving mechanical strength [3], thus can be present in cementitious pore water in significant concentrations ($[Gluc^-] \leq 10^{-2}$ M [4]). The characteristics of sodium gluconate to enhance the solubility of tri-, tetravalent actinides, and lanthanides have been studied in acidic and neutral media [5,6] but rarely in alkaline equilibria [7–9].

The radiotoxicity of spent nuclear fuel is predominated by actinides (Am^{3+}, Cm^{3+}, Pu^{3+}, and Pu^{4+}) in radioactive waste repositories [10], where anoxic conditions are typical [11], ensuring that reduced oxidation states of actinides prevail under these conditions [10–13]. The formation of hydroxo- and carbonato- complexes of radioactive actinides increase solubility [10], which can be further enhanced by complexation of gluconate present [9]. In the case of groundwater infiltration to the repository, to know the degree of mobilization these metal ions can reach is essential to calculate the associated risk of the disposal [10].

To obtain a simplified and relevant model of all possible processes of complex formation, tri- and tetravalent actinides can be modeled by less elaborate lanthanide ions, such as neodymium (Nd^{3+}) [14]. This replacement is reasonable due to the pronounced chemical analogies stable 3+ oxidation state lanthanide ions share with trivalent actinides [15], and the fact that ionic radii shows only slight changes in the case of Nd^{3+}, Pu^{3+}, Am^{3+}, and Cm^{3+} [16,17], which ensures similar properties for the coordination compounds [18]. Furthermore, due to its availability, safe usage, and the sensitivity of its visible spectrum to coordination, neodymium can be a suitable radioactive surrogate of actinides

* Corresponding author at: Department of Inorganic and Analytical Chemistry, University of Szeged, Dóm tér 7, H-6720 Szeged, Hungary.
E-mail addresses: boseva@chem.u-szeged.hu (É. Böszörményi), kasa.zsolt@chem.u-szeged.hu (Z. Kása), gabor.varga5@chem.u-szeged.hu (G. Varga), kele.zoltan@med.u-szeged.hu (Z. Kele), kutusb@mpip-mainz.mpg.de (B. Kutus), peintler@chem.u-szeged.hu (G. Peintler), sipos@chem.u-szeged.hu (P. Sipos).
† Deceased.

https://doi.org/10.1016/j.molliq.2021.117047
0167-7322/

in coordination chemistry [16]. The visible light spectra have been successfully utilized to study a variety of coordination compounds [19–22], considering that the hypersensitive transitions of Nd^{3+} $^4I^4_{9/2}\rightarrow G_{5/2}$, $^2G_{7/2}$ are found between 545.0 and 605.0 nm [19]. Zanonato *et al.* found that NdL_x (L: ligand, x = 1, 2, 3) complexes form in the case of an acetate ligand, and stronger complex formation is typical at elevated temperatures [20]. When a more comprehensive *p*H range (5–11) was studied, Nd^{3+} was found to express a significant red shift upon deprotonation and complexation of D-glucosamine [22], and precipitation appeared at *p*H > 8.6 at several different metal to ligand ratios [22]. Levitskaia *et al.* referred to the precipitation as $Nd(OH)_3$ [22] since Nd^{3+} is known to form insoluble $Nd(OH)_3$ around *p*H = 8 [23–25]. Collaterally, a precipitate appeared in the case of the praseodymium-gluconate system at *p*H = 8 [8] when the ligand to metal ratios were lower than 2:1. In both cases, it was noted that increasing ligand excess would result in the precipitate forming at higher *p*H [22] or appear delayed [8].

Giroux *et al.* reported that given the same conditions, precipitate also appears in the case of La^{3+}, Eu^{3+}, Dy^{3+}, Er^{3+}, and Lu^{3+} ions around *p*H = 8 or at slightly higher *p*H when $Gluc^-$ is in excess [7]. In their study, seven complexes were described to form with all the five studied lanthanide cations: ML^{2+}, MLH^+_{-1}, MLH_{-2}, ML^+_2, ML_2H_{-1}, $ML_2H^{2-}_{-3}$, and $M_2L_2H^-_{-5}$ from which MLH_{-2} becomes predominant at pH 8–10 [8]. Kutus *et al.* found that in the Nd^{3+}–$Gluc^-$ system, one complex forms at the same *p*H with the same composition: $NdGlucH_{-2}$ [26], and a precipitate appears at *p*H = 8, which was proven to have the composition of $NdGlucH_{-1}OH$ in our previous work [27]. However, precipitation does not occur in the Nd^{3+}–$Gluc^-$ system at *p*H > 12, which raises concerns of increased solubility since the complex formation was scarcely studied at *p*H higher than twelve [9,28], although this hyperalkaline medium [10] and high ionic strength (I = 5.3–7.4 M) [11] is inherent to radioactive depositories. Considering that Kutus *et al.* proved the formation of polynuclear Nd^{3+}–$Gluc^-$ complexes as *p*H increases [26] and Giroux *et al.* reported that lanthanides tend to form $M_2L_2H^-_{-5}$ in alkaline media, the redissolving precipitate implicates that dimer or polynuclear complexes can be present in hyperalkaline medium which is also foreshadowed by the characteristic of Nd^{3+} to dimerize even as hydroxide in $Nd_2(OH)^{4+}_2$ form [29].

Our aim was to present further data about complexes forming in highly alkaline media at high ionic strengths. Both of these conditions are extreme occurrences related to radioactive repositories [2,3], and the complexation of lanthanides and actinides have rarely been studied in extremely alkaline media [9,28]. Better understanding of the Nd^{3+}–$Gluc^-$ system under these conditions contributes to a comprehensive model of lanthanides' chemical behavior, which could be further utilized when the mobilization of actinides is calculated to provide a more reliable interpretation of these systems.

2. Experimental section

2.1. Materials and solutions

For the preparation of solutions, sodium-D-gluconate (Sigma, ≥99%) was used as received. Neodymium(III) chloride hexahydrate (Alfa Aesar, ≥99.9%) was dissolved in deionized water, then filtered to remove colloid $Nd(OH)_3$. The exact analytical concentration of the $NdCl_3$ solution was determined by EDTA titration by using methylene blue as an indicator, based on a method reported previously [26]. The titrant for calibrations were approximately 2.0 M stock solutions of NaOH at 4.5 M ionic strength, prepared by diluting freshly filtered ~ 20 M NaOH (Analar Normapur). The exact concentrations were determined *via* titrating standardized HCl solution. For reverse titrations, an approximately 1.0 M stock solution of HCl at 4.5 M ionic strength was prepared by volumetric dilution of concentrated HCl (*ca.* 37% w/w, VWR). Its exact concentration was determined *via* titrating a solution of dried $KHCO_3$ using methyl orange as indicator. All stock solutions and samples were prepared using deionized water (Merck Millipore Milli-Q), and the ionic strengths were adjusted by using NaCl (Acros Organics, ≥99%).

2.2. Potentiometric titrations

Potentiometric titrations were carried out at constant ionic strength of 4.0 M, using a Metrohm 888 Titrando instrument attached to a platinized platinum electrode and a thermodynamic Ag/AgCl reference electrode. Bubbling high purity H_2 gas excluded CO_2 from the titration cells. The electrochemical cell was constructed as follows:

$$H_2/Pt \mid \text{test solution, I = 4 M (NaCl)} \parallel 4\ M\ NaCl \mid 4\ M\ NaCl, Ag/AgCl$$

Cell calibrations were performed in the 1.0 < *p*H (defined as $-\log([H^+]/c^\ominus$, where $c^\ominus = 1$ M) < 13.5 range, 0.1 M HCl, and 0.05 M malonic acid solutions were titrated at 4.0 M ionic strength. Within the range, the cell response was linear and exhibited 59.1 ± 0.2 mV slope. The applied calibration method is detailed in the manual of the *p*HCali software [30].

The titration cell was thermostatted to 25.0 ± 0.1 °C (Julabo F12-MB thermostat). Potentiometric titrations of solutions containing both $NdCl_3$ and NaGluc were performed. The total concentration of $NdCl_3$ was varied between 0.05 and 0.15 M; the titrations were carried out at 1:2.5–1:4 metal to ligand ratios. The initial total concentration of NaOH was 0.8 M in each titrated solution, the titrant was 1.0 M HCl solution, and the ionic strength was set to 4.0 M with NaCl. The obtained data were evaluated using the program PSEQUAD [31]. The autoprotolysis constant of water at I = 4.0 M ionic strength (pK_w = 14.26 ± 0.02) was previously determined [32].

In accordance with our previous publication [25], precipitation occurs in the Nd^{3+}–$Gluc^-$ system at *p*H > 8, but precipitation disappears at *p*H > 12 if the metal to ligand ratio is at least 1:2.5. The appearing precipitate was studied previously [27], and its composition was constant in the *p*H = 8 – 12 range. Based on these data, potentiometric measurements were carried out in a reversed manner (titrating a *p*H ≈ 13.5 sample with 1.0 M HCl (I = 4.5)) to reveal the interactions that take place in alkaline Nd^{3+}–$Gluc^-$ solutions.

2.3. Spectrophotometry

The spectra were recorded on an Analytik Jena Specord 210 Plus 190(UV/Vis)-1100 nm double beam spectrophotometer, in the wavelength range of 200–900 nm. A standard quartz cuvette was used for all measurements (optical path length: 1 cm). Every sample was thermostatted and measured at room temperature (25.0 ± 0.1) °C at 4.0 M ionic strength. Several sets of samples were measured; $[NaOH]_T$ (hereafter the subscript T denotes total or analytical concentration) was varied between 0.2 and 1.0 M while the metal to ligand ratio was fixed between 1:2.5 – 1:4.0. If the *p*H > 12 conditions are met, precipitation does not occur in the solutions, and this condition also excludes the lactonization of D-gluconic acid [33,34]. The spectra in the 445 – 900 nm range were evaluated by Matrix Rank Analysis (MRA) [35] to determine the number of colored complexes were present in our system. Furthermore, the UV–Vis data were inserted into the PSEQUAD model, which contained the potentiometric titrations. The molar absorption coefficient — calculated from independent calibrations — was found to be 6.70 ± 0.02 M^{-1} cm^{-1} at 575 nm.

2.4. Freezing-point depression

Freezing-point depression measurements were performed using a Testo 735 digital precision thermometer, to further confirm results obtained *via* other methods. The probe has an accuracy of ± 0.05 °C. The freezing-point depression was calculated comparing it to that of distilled water, and the coolant was 5.0 M NaCl at − 20 °C. Freezing points were measured and corrected by the freezing point of deionized water (used as a reference point). The corresponding temperature was determined *via* undercooling samples, measuring ice nucleation temperature in equilibrium with the liquid phase. The measured samples consisted of $[NdCl_3]_T$ = 0.050–0.150 M, and the metal to ligand ratio was kept at 1:2.5 in each sample. The concentration of sodium-hydroxide was set to $[NaOH]_T$ = 0.300 M in the case of $[NdCl_3]_T \leq 0.100$ M and $[NaOH]_T$ = 0.400 M in the case of $[NdCl_3]_T \geq 0.100$ M. The ionic strength was not adjusted in this case, since NaCl affects freezing point depression, and the effect of excess NaCl present in the solutions was taken into account.

2.5. Electrospray ionization mass spectrometry (ESI-MS)

A Q Exactive Plus hybrid quadrupole-orbitrap mass spectrometer (Thermo Scientific, Waltham, MA, USA) equipped with a heated electrospray ionization (HESI-II) probe was used to record the MS spectra both in positive and in negative ion mode. Samples were introduced by flow injection analysis method, the eluent stream (water, acetonitrile in 1:1 vol ratio) was provided by a Waters Nano Acquity UPLC system. Samples were prepared using D-(+)-Gluconic acid δ-lactone (Fluka chemika, ≈99%) and 0.1 M $Nd(NO_3)_3$ solution, prepared by dissolving $Nd(OH)_3$ (Sigma, ≥ 99.995%) in HNO_3 (Sigma Aldrich, ≥9 9.9%). The pH of samples was set by adding NH_3 (≈25 % m/m, Molar chemicals).

2.6. Nuclear magnetic resonance (NMR)

^1H and ^{13}C NMR spectra were recorded on a Bruker Avance III HD 500 MHz NMR spectrometer employing a 5 mm inverse broadband probe head (CryoProbe™Prodigy) furnished with z-oriented magnetic field-gradient capability. Solvent suppression was not applied, and the baseline was subtracted from each spectrum numerically. *Prior to* any measurement, the magnetic field was locked to the 2D signal of the solvent for stabilization. The temperature was 25 ± 1 °C, 10% (V/V) D_2O was added to each sample, while the ionic strength was not adjusted in this case. The solutions were prepared to study the effect of metal ion on the ligand spectra. The concentration of NaGluc was fixed at $[NaGluc]_T$ = 0.100 M, and $[NdCl_3]_T$ was increased from 0.001 M to 0.040 M. The *p*H was set to 13, respectively, and 128 and 512 interferograms were collected to obtain the ^1H and ^{13}C NMR spectra.

2.7. Raman spectroscopy

Raman spectra with 4 cm^{-1} resolution were recorded using a Raman Senterra II (Bruker) microscope. For each spectrum, 2048 scans were accumulated upon using exposition time of 10000 ms, using a laser of 532 nm wavelength with an intensity of 25 mW. The objective magnification was 50, while the integration time was 50 s.

2.8. Data processing

The complexation reaction between Nd^{3+} and $Gluc^-$ ions can be generally described as follows:

$$pNd^{3+} + qGluc^- + rH^+ \rightleftharpoons Nd_pGluc_qH_r^{(3p-q+r)} + rH_2O \quad (1)$$

$$\beta_{pqr} = \frac{[M_pL_qH_r]}{[M]^p[L]^q[H^+]^r(c)^{1-p-q-r}} \quad (2)$$

where $c^{ø}$ is the standard molar concentration of unity, $c^{ø}$=1 M. The stability constants and the molar absorptivities of the species forming were calculated for potentiometric and spectrophotometric data with the aid of the PSEQUAD [31] software. The aim of the fitting procedure is to minimalize the fitting parameter (FP):

$$FP = \sum_{q=1}^{n_d} FP_q = \sum_{q=1}^{n_d}\sum_{i=1}^{r_q}\left(\omega_1\left(\Delta X_1^V\right)^2 + \sum_{k=2}^{m}\omega_k\left(\Delta X_k^p\right)^2 + \omega_A\sum_{k=m+1}^{p}\left(\Delta X_k^A\right)^2\right) \quad (3)$$

where n_d is the number of sets of measurements derived from different types of primary experimental data, r_q is the number of experimental points in the qth set of measurements, ω_1 is the weighting factor of the volume of the titrant or total concentrations, ω_k is the weighting factor for the kth potential measurements, and ω_A is the weighting factor for the absorbance measurements.

3. Results and discussion

3.1. Potentiometric and UV–Vis spectroscopic data analysis

To create a model, which describes the complexes present in the system adequately, first potentiometric and spectrophotometric measurements were carried out.

The titration curves (Fig. 1.) attest a pronounced metal concentration dependence, suggesting the formation of polynuclear complexes. The absence of inflection points could be ascribed to the narrow *p*H range inspected. While the potentiometric measurements suggest that the complex formation is heavily affected by metal concentration, the Vis-NIR spectra registered show *p*H dependence. Potentiometric and spectrophotometric measurements were carried out in the same concentration range resulting in more empirical information about the Nd^{3+}– $Gluc^-$ system.

The absorbances (Fig. 2.) in the hypersensitive region (around 580 nm) as well as the other peak at around 800 nm slightly red shifted with increasing $[NaOH]_T$. The extent of this effect is far beyond the uncertainty of the experimental method and likely to indicate complex formation. The absence of one single isosbestic

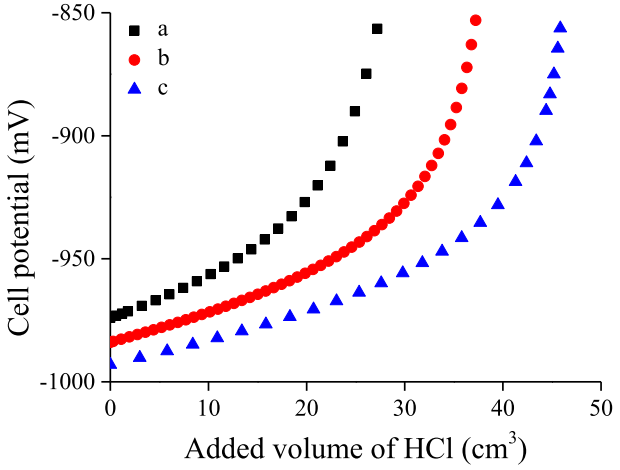

Fig. 1. Potentiometric curves of reverse titrations in the Nd^{3+}–$Gluc^-$ system. Symbols denote the measured cell potential values. Experimental conditions: T = 25 °C, I = 4 M (NaCl). Exact reactant concentrations used for the titration curves a, b and c are shown in Table 1.

Table 1
Initial total concentrations of samples and the titrant HCl solution corresponding to the graph in Fig. 1.

Sample	$[NdCl_3]_{T,0}$/M	$[NaGluc]_{T,0}$/M	$[NaOH]_{T,0}$/M	c_{HCl}/M
a	0.1557	0.3908	0.7952	1.009
b	0.1013	0.3053	0.7913	1.009
c	0.04954	0.1483	0.7909	0.9906

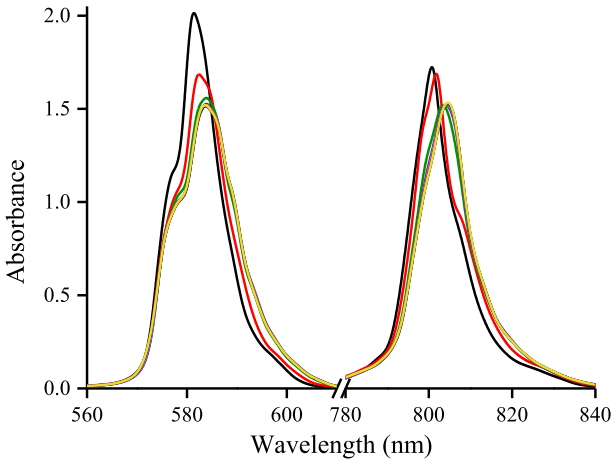

Fig. 2. Effect of increasing $[NaOH]_T$ on the visible spectra of the Nd^{3+}–$Gluc^-$ system. Experimental conditions: T = 25 °C, I = 4 M (NaCl); analytical concentrations: $[NdCl_3]_T$ = 0.09910 M, $[NaGluc]_T$ = 0.3000 M, $[NaOH]_T$ changes from 0.1988 M (black spectrum) to 0.9938 M (yellow spectrum) in *ca.* 0.1 M increments.

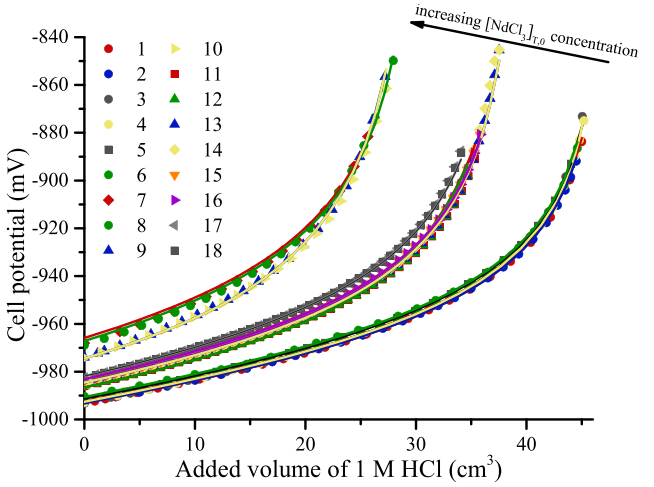

Fig. 3. Potentiometric curves of reverse titrations in the Nd^{3+}–$Gluc^-$ system. Experimental conditions: T = 25 °C, I = 4 M (NaCl); *p*H is varied between 13.8 and 12.5. Symbols: measured, lines: calculated data. Analytical (or total) concentrations of the titrated samples are shown in (ESI) Table S1.

point shows the formation of more than two deprotonated Nd^{3+}–$Gluc^-$ complexes. Matrix rank analysis, based on these spectrophotometric data, suggests that at least three, but not more than five different colored complexes are present. To identify these complexes, the conventional fitting procedure was carried out using the PSEQUAD program [31] and employing an extended set of chemically meaningful species in every possible combinations, which meant the testing of several hundred different models. At first, only the potentiometric data were fitted to acquire an incipient description of the system; during these calculations, the results of the MRA were taken into consideration, as limiting condition. As a next step, simultaneous fitting of the potentiometric and spectrophotometric data was used, to improve the accuracy of the stability constants determined and to obtain a reasonable chemical model.

Model selection was first based on trivial mononuclear complexes, but in this case, although several plausible combinations with different Nd^{3+}:$Gluc^-$:OH^- ratios were systematically included during fitting, systematic differences occurred between the observed and calculated data, especially at higher metal ion concentrations. This hints that besides the mononuclear complexes, polynuclear ones may also be present in the solution; consequently, complexes containing two neodymium ions were included into the model. It was observed that the inclusion of even one binuclear complex in the model improved the agreement between the observed and calculated titration curves.

Besides the one binuclear $Nd_2Gluc_4H_{-6}^{4-}$, complex, including its other protonated form $Nd_2Gluc_4H_{-5}^{3-}$ and two other binuclear complexes, $Nd_2Gluc_6H_{-4}^{4-}$ and $Nd_2Gluc_6H_{-5}^{5-}$ reasonably improved the model to account for the observed potential values. Adding the $NdGluc_2H_{-5}^{4-}$ mononuclear complex to the model resulted in good agreement between the measured and calculated values within the experimental uncertainty (Fig. 3).

The necessity of describing the system using four binuclear complexes in the model is highlighted when Fig. 3 and Supporting Information (ESI) Figures S1–S3 are compared. In Fig. 3, the average difference between the fitted and observed titration curves was found to be 1.34 mV, and the curvatures of the titrations are well reproduced. This, however, in itself would not explain why binuclear complexes are necessary to include for obtaining the accurate model. ESI Figure S1 clearly illustrates that including only the two $Nd_2Gluc_4H_{-6}^{4-}$ and $Nd_2Gluc_4H_{-5}^{3-}$ binuclear species in the speciation model results in a reasonably acceptable fit, further improved by adding the other two binuclear complexes (ESI Figs. S2) and (the expected) mononuclear complex to the fitted model. Moreover, including the mononuclear complex to be present in the model, the slight and systematic differences between the calculated and experimental curves' structure were significantly improved (ESI Figures S2 and S3). The stability constants of the mono- and binuclear complexes are shown in Table 2.

Experimental data suggest that the occurring precipitation, $NdGlucH_{-1}OH$ redissolves at *p*H = 12 in the form of $Nd_2G_4H_{-5}^{3-}$ binuclear complex, which goes through two subsequent deprotonation steps as the $[NaOH]_T$ increases and mononuclear complexes become predominant only at *p*H > 13. The distribution diagram calculated and plotted using the lgß values obtained in this work is depicted in Fig. 4. In our previous work, the formation of a neutral binuclear complex bearing the same M:L ratio as $Nd_2Gluc_4H_{-2}^{4-}$, $Nd_2Gluc_4H_{-2}^{0}$ has been described already at *p*H = 6.5, which could corroborate the dimerization in alkali solutions [26]. Giroux *et al.* found that several lanthanides exhibit the same characteristics; La^{3+}, Eu^{3+}, Dy^{3+}, Er^{3+}, and Lu^{3+} cations were all proven to form $M_2L_2H_{-5}^{-}$, complexes, alongside ML^{2+}, MLH_{-1}^{+}, ML_2^{+}, ML_2H_{-1}, and $ML_2H_{-3}^{2-}$ [7] (here L stands for various polyhydroxy carboxylic acids, including $Gluc^-$).

Giroux *et al.* also found that in acidic media, two main species, ML and ML_2 are present, and the complexes deprotonate as *p*H increases [7,8]. Similarly to this, in our system $Nd_2Gluc_6H_{-4}^{4-}$ is present at *p*H = 10 and deprotonates as the $[OH^-]$ concentration gets higher, and $NdG_2H_{-5}^{4-}$, which can be described as $Nd(OH)_3$ stabilized by $Gluc^-$ in solution, dominates the highest *p*H range. The existence

Table 2
Stability constants of the species present in alkaline solutions containing Nd^{3+} and $Gluc^-$ at T = 25 °C and I = 4 M (NaCl).

Reaction	lgβ	std. dev.
$Nd^{3+} + 2Gluc^- = NdG_2H_{-5}^{4-} + 5H^+$	−58.76	0.03
$2Nd^{3+} + 4Gluc^- = Nd_2G_4H_{-5}^{3-} + 5H^+$	−47.57	0.07
$2Nd^{3+} + 4Gluc^- = Nd_2G_4H_{-6}^{4-} + 6H^+$	−60.02	0.07
$2Nd^{3+} + 6Gluc^- = Nd_2G_6H_{-4}^{4-} + 4H^+$	−35.38	0.07
$2Nd^{3+} + 6Gluc^- = Nd_2G_6H_{-5}^{5-} + 5H^+$	−46.57	0.07

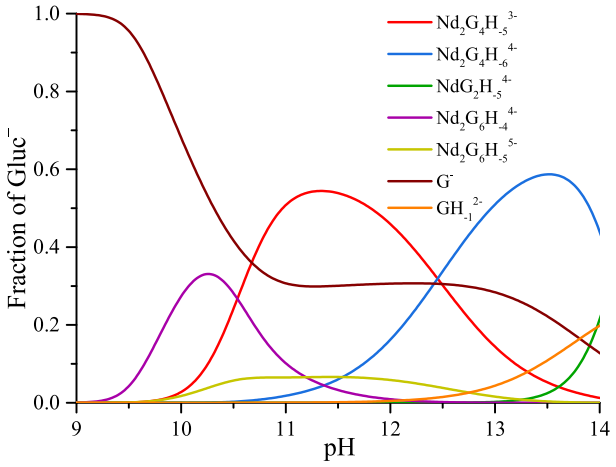

Fig. 4. Distribution diagram of the neodymium-gluconate binary system, presuming $[Nd^{3+}]_T$ = 0.1000 M and $[Gluc^-]_T$ = 0.3000 M concentrations.

of $Nd_2Gluc_6H_{-4}^{4-}$ and $Nd_2Gluc_4H_{-5}^{3-}$ and their two other deprotonated forms reflect the affinity of Nd^{3+} to dimerize: even as a hydroxido complex, the metal ion is known to form $Nd_2(OH)_2^{4+}$ [29]. Although polynuclear complexes have only been reported by Giroux *et al.* [7] and Kutus *et al.* [26], several examples of lanthanide-gluconate mononuclear complexes have been described under *p*H = 8 in the literature, *e.g.,* for Pr^{3+} [8], Eu^{3+} and Am^{3+} [9], as well as Nd^{3+} [26,35]. The usually employed low concentrations of Nd^{3+} and $Gluc^-$ in previous solubility studies of trivalent actinides/ lanthanides could also explain the lack of multinuclear complexes reported in alkaline solution, since in our study the reactant concentrations were significantly higher.

Simultaneous evaluation of the absorption spectra further confirmed the five complexes described above. It needs to be emphasized that assuming only the two binuclear species $Nd_2Gluc_4H_{-6}^{4-}$, and $Nd_2Gluc_4H_{-5}^{3-}$ provided an almost acceptable interpretation of the potentiometric data; therefore, these complexes are essential for constructing of a reasonable model. Furthermore, from the UV–Vis spectroscopic data, the PSEQUAD program could determine the molar absorptivities of the fitted particles, which could provide more information from the formed complexes. Calculated molar absorptivities (Fig. 5.) show that a bathochromic shift is induced upon deprotonation of complexes, and molar absorptivities of binuclear complexes are roughly doubled compared to the mononuclear complex. Observations similar to these were obtained for solutions with acidic pH by Kutus *et al.* [25]. Molar absorptivities of species at the peak around 804 nm are depicted in ESI Fig. S4., affirming the bathochromic shift upon further deprotonation.

3.2. Model validation

3.2.1. Freezing point depression

Additional experimental data were collected to confirm the formation of complexes in the solutions studied. First, freezing-point depressions of selected solutions were determined (Table 2), then

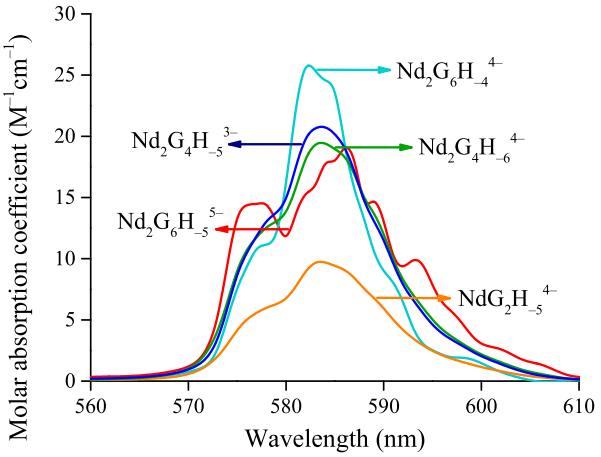

Fig. 5. Molar absorption spectra of the mononuclear and binuclear neodymium complexes in the hypersensitive region of neodymium.

freezing-point depressions of the solutions were calculated as follows

$$\Delta T_f = T_{f(pure\,solvent)} - T_{f(solution)} = K_f \hat{A} \cdot m_B \quad (4)$$

where theoretical freezing point depression (ΔT_f) is proportional to the concentration of the fully dissociated species, K_f is the cryoscopic constant (1.86 K·kg/mol for water), and m_B is the molality of the solute, which can be replaced by molar concentration values in relatively dilute solutions. According to the colligative property of freezing point depression, it decreases upon complexation when the number of solute particles decreases due to, *e.g.,* complex formation.

The measured freezing-point depression values of the first six solutions (ΔT_{meas}) are identical to those calculated assuming total dissociation (ΔT_{tot}). The remaining solutions were all binary systems containing Nd^{3+} and $Gluc^-$ at a *p*H higher than 12. Complexes are expected to be present in reasonably large concentrations in these solutions, which accounts for explaining why the registered freezing point depression values are smaller than the theoretical values when total dissociation is assumed (Fig. 6.). This observation suggests that complexation takes place in the system. When freezing point depression values are calculated (ΔT_{calc}) using the formation constants presented in Table 3, the agreement between the observed and predicted values is reasonably good. The minute differences between the ΔT_{meas} and ΔT_{calc} values are most probably associated with the fact that the ionic strength of these solutions could not be adjusted to 4.0 M due to the nature of such measurements.

3.2.2. ESI-MS

ESI-MS measurements were performed to further confirm the complexation processes observed in the studied system. The spectra of several samples containing both Nd^{3+}, $Gluc^-$, and NH_3 (latter provided the basic conditions) were recorded in positive and negative ion mode. Neutral complexes do not show up in the mass spectra; only charged species can be detected in positive or negative ion mode. Free $Gluc^-$ for example, shows up as a distinctive peak in a spectrum registered in negative ion mode, while the described species having lower negative charges like 2−, 3 − or even 4 − usually gain positive charge(s) *via* "binding" protons or Na^+. Because of these highly negative charges, appraising the exact molecular weight becomes problematic since several association processes can occur during the measurement time. While deducing the exact composition of the detected species was not possible, in positive ion mode peaks corresponding to the mononuclear com-

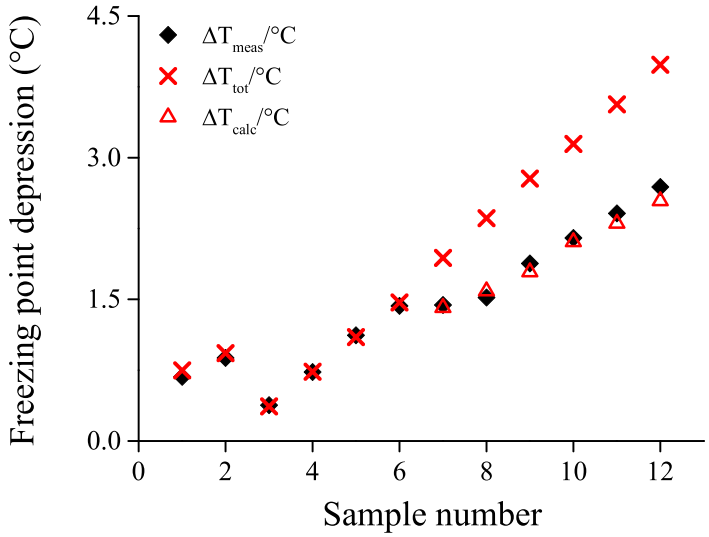

Fig. 6. Comparison of the measured and calculated freezing point depression values to validate the suggested speciation model presented in Table 3.

Table 3
Composition of the solutions studied with freezing point depression. ΔT_{meas} is the measured freezing point value, ΔT_{tot} is the computed freezing point depression assuming total dissociation of the species, ΔT_{calc} is the calculated freezing point value based on the model derived from the fitting of the potentiometric and spectrophotometric measurements. The first six solutions were strong electrolytes; therefore, freezing point depressions were not calculated in their case.

#	$[Nd^{3+}]_T$ /M	$[Gluc^-]_T$ /M	$[OH^-]_T$ /M	ΔT_{meas}/°C	ΔT_{tot}/°C	ΔT_{calc}/°C
1	0.1006	0.0000	0.0000	0.68	0.75	
2	0.0000	0.2500	0.0000	0.88	0.93	
3	0.0000	0.0000	0.0986	0.38	0.37	
4	0.0000	0.0000	0.1971	0.73	0.73	
5	0.0000	0.0000	0.2957	1.12	1.10	
6	0.0000	0.0000	0.3943	1.43	1.47	
7	0.0503	0.1250	0.2957	1.44	1.94	1.41
8	0.0754	0.1875	0.2957	1.52	2.36	1.59
9	0.1006	0.2500	0.2957	1.88	2.78	1.79
10	0.1006	0.2500	0.3943	2.15	3.14	2.11
11	0.1257	0.3125	0.3943	2.41	3.56	2.30
12	0.1509	0.3750	0.3943	2.69	3.98	2.54

plex $NdGluc_2H_{-5}^{4-}$ showed up on the ESI-MS spectra displaying the unique isotope distribution characteristic to Nd^{3+} at 804.34 *m*/*z* values (ESI Fig. S5) confirming the presence of the NdGluc complexes in the solution.

3.2.3. Nuclear magnetic resonance

Because of the interaction between the unpaired electrons and the NMR active nucleus studied, lanthanides can induce sizeable paramagnetic shift and significant peak broadening in the NMR spectra. This effect has already been studied for several paramagnetic ions complexed with $Gluc^-$, such as Nd^{3+} [36], Dy^{3+} [7], Pr^{3+} [8], Mn^{2+} and Co^{2+} [37] since the markedly greater degree of shifting and broadening of certain signals is suited for identifying the binding sites of the ligand.

To gain structural insight into the complexes forming, a series of ^1H and spectra as a function of $[Nd^{3+}]_T$ at *p*H = 13 were recorded. When the concentration of $NdCl_3$ is increased from 0.005 to 0.020 M in solutions containing constant 0.1 M NaGluc, the complexation of Nd^{3+} by $Gluc^-$ causes a general peak shift and broadening even at the highest ligand to metal ratio (Fig. 7).

This shift could be described by assuming the formation of deprotonated complexes, which imply a stronger interaction between the paramagnetic metal center and the ligand. Remarkable signal widening appears in the spectra for the peaks of H2 and H3 nuclei, suggesting that these forming alcoholate groups can be effective binding sites upon deprotonation. The ^1H and ^{13}C

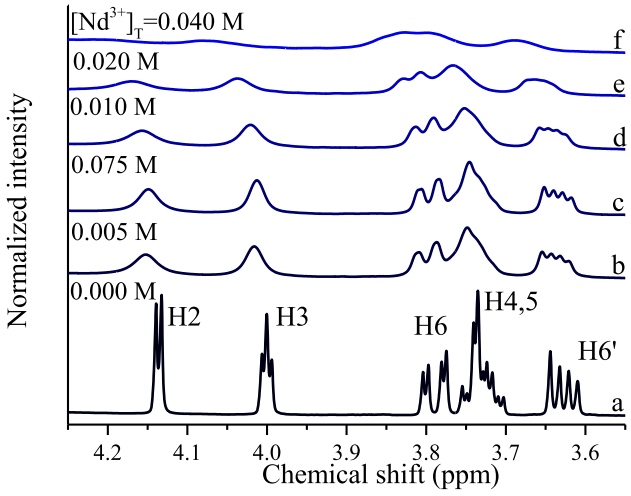

Fig. 7. NMR spectra as a function of increasing $[Nd^{3+}]_T$ at *p*H = 13. $[Gluc^-]$ = 0.1000-M was kept constant.

peak assignments of $Gluc^-$ were reported in the literature previously [38,39], and Akhmetov *et al.* has reported that the structure of $Gluc^-$ does not depend on its concentration significantly. Coordination indicated at C2 alcoholate group of $Gluc^-$ has been

reported by Giroux *et al.* regarding Pr^{3+} and Dy^{3+} [7], while regarding Eu^{3+}–Gluc [5] and Ca^{2+}–Gluc [39] complexes, the C3 alcoholate group was also suggested as biding site. These spectral variations can be ascribed to the species for which the main coordination sites are the carboxylate and the OH group attached to the C2 and C3 carbon atoms. The identified coordination sites are supported by the ^{13}C NMR spectrum of 0.1 M NaGluc and 0.005 M $NdCl_3$ (Fig. S10) since the intensities of the C1 and C2 peaks decrease significantly.

3.2.4. Raman spectroscopy

Raman spectroscopy is a suitable vibration spectroscopic technique for directly identifying interactions between $Gluc^-$ and metal ions, like Nd^{3+}, in aqueous solutions. The Raman spectra of the pure NaGluc and that of two further neodymium-containing NaGluc solutions are shown in Fig. 8. Band assignment are presented in Table 4. As can be seen in all Raman spectra, four relatively broad intense peaks appear in the range of 1150–750 cm^{-1} represented carbohydrate framework of $Gluc^-$ [40]. The most intense peak (~1100 cm^{-1}) was assigned (as for all saccharides) to bending mode vibrations of C(1)–H and C–OH groups [41]. By increasing the concentration of neodymium this vibration band becomes distorted, and a new band appears at 1054 cm^{-1}. This process might be related to the deformation of the $Gluc^-$ skeleton. The coordination of Nd^{3+} onto hydroxyl group(s) might have a similar or the same impact on the $Gluc^-$ framework.

Table 4
Assignment of Raman vibration bands of NaGluc in aqueous solution.

Band position (cm^{-1})	Assignment	References
1645	$\nu_{asym}(COO^-)$	[40,43]
1463–1469	$\omega(CH_2)$	[40,41]
1408–1410	$\delta(CH) + \delta(OH)$	[40,41]
1356	$\nu_{sym}(COO^-)$	[40,43]
1310	$\nu_{sym}(COO^-)$	[40,43]
1095–1100	$\delta(C(1)–H) + \delta(C–OH)$	[42,43]
950–960	$\delta(C–H) + \delta(C–OH)$	[42,43]
880–885		
800–810		

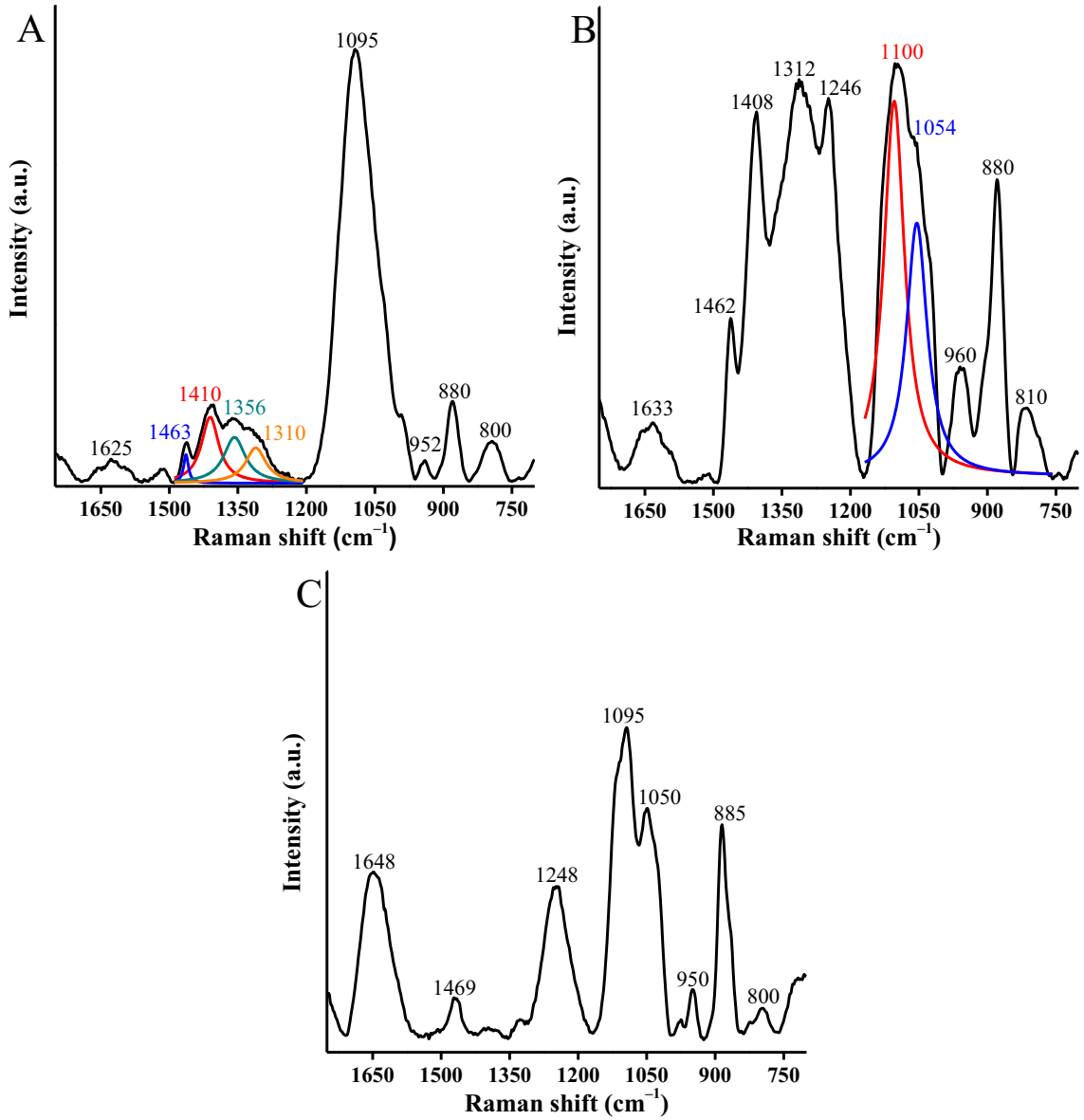

Fig. 8. Raman spectra of a $[NaGluc]_T$ = 2.7 M solution at pH = 7.0 (A); a solution with gluconate-excess ($[NaGluc]_T$ = 2.0 M and $[NdCl_3]_T$ = 0.8 M) at pH = 13.0 (B) and a solution with neodymium-excess ($[NaGluc]_T$ = 0.5 M and $[NdCl_3]_T$ = 2.0 M) at pH = 4.0 (C).

Furthermore, three other bands (952 cm^{-1}, 880 cm^{-1} and 800 cm^{-1}) were exhibited in the spectrum of NaGluc in this frequency range, which can be identified as other different bending mode vibrations of C(1)–H and C–OH groups [42]. These were invariable peaks and independent of the metal ion concentration and solution conditions. In the high energy region, the first peak (1463 cm^{-1}) with medium intensity was attributed to CH_2 bending mode vibration, with unchanged position but with reduced intensity upon complexation [42]. Similarly, bending of CH and OH groups exhibited a single peak at about 1410 cm^{-1}, which also decreased in intensity upon interacting with Nd^{3+} [42]. Additional two peaks (1356 cm^{-1} and 1310 cm^{-1}) correspond to the symmetrical stretching mode of the carboxylate group. Its asymmetrical vibration band was also seen at 1630 cm^{-1} with very weak intensity, similarly to many carboxylates [40,43].

Due to the possible impact of coordinated Nd^{3+} centers on the microstructure of the carboxylate group, symmetrical carboxylate group vibrations were shifted significantly towards the lower wavenumber region (1312 cm^{-1} and 1246 cm^{-1}). On one hand, taking into account the empirical law on the separation of carboxylate bands ($\Delta = \nu(COO^-)_{asym.} - \nu(COO^-)_{sym.}$) [44,45], monodentate coordination mode of carboxylate group onto Nd^{3+} ions could be assumed based on the increased separations each solution with complexes ($\Delta_{complex}$ = 321 cm^{-1} and 387 cm^{-1} for system (B) or 400 cm^{-1} for system (C) in Fig. 8.) compared to the one in sodium gluconate solution (Δ_{salt} = 269 cm^{-1} and 315 cm^{-1}). Relative to the Nd^{3+}-free systems, the two well-separated symmetrical carboxylate vibration bands were retained in presence of lower concentration of Nd^{3+} and in high *p*H solution, which might reflect the formation of monodentate as well as bridging type coordination mode of the carboxylate group [45], similar to that seen in the structure of the $Cu_2(OAc)_4{\cdot}2H_2O$ complex [46]. In presence of Nd^{3+}-excess and at acidic *p*H, only one symmetrical carboxylate vibration band could be observed at 1248 cm^{-1}, due to the dominance of monodentate coordination under these experimental conditions [45]. It was somewhat surprising to note that the intensity of the asymmetric vibration band of the carboxylate group increased with increasing neodymium concentration. Additionally, a slight shift can be experienced in the position of that particular band in the spectrum of the Nd^{3+} containing solutions relative to the pure $Gluc^-$ solution indicating the change in the first coordination sphere of Nd^{3+}. The deconvoluted spectra with the fitted curves can be found in the Supporting Information (Fig. S6–S8.).

4. Conclusions

The UV–Vis spectrum of the Nd^{3+} aqua ion does not express significant shifts in highly alkaline media but when they are evaluated together with potentiometric data, the Nd-Gluc system can be accurately described. Fitting the spectrophotometric and potentiometric experimental data simultaneously, the formation of four binuclear and one mononuclear species ($Nd_2Gluc_4H_{-5}^{3-}$, $Nd_2Gluc_4H_{-6}^{4-}$ $Nd_2Gluc_6H_{-4}^{4-}$, $Nd_2Gluc_6H_{-5}^{5-}$ and $NdGluc_2H_{-5}^{4-}$) were detected. This confirms the presence of polynuclear complexes suggested in earlier studies.

CRediT authorship contribution statement

Éva Böszörményi: Data curation, Formal analysis, Investigation, Methodology, Validation, Visualization, Writing - original draft. **Zsolt Kása:** Investigation, Methodology, Software. **Gábor Varga:** Investigation, Validation. **Zoltán Kele:** Investigation, Validation. **Bence Kutus:** Conceptualization, Formal analysis, Investigation, Supervision, Validation, Visualization, Writing - review & editing. **Gábor Peintler:** Data curation, Formal analysis, Software. **István Pálinkó:** Conceptualization, Funding acquisition, Project administration, Resources, Supervision, Writing - review & editing. **Pál Sipos:** Conceptualization, Funding acquisition, Project administration, Resources, Supervision, Writing - review & editing.

Declaration of Competing Interest

The authors declare that they have no known competing financial interests or personal relationships that could have appeared to influence the work reported in this paper.

Acknowledgments

This research was funded by the National Research Development and Innovation Office, Grant number (NKFIH K 124265). Zsolt Kása acknowledges the financial support of the NTP-NFTÖ scholarship.

Appendix A. Supplementary data

Supplementary data to this article can be found online at https://doi.org/10.1016/j.molliq.2021.117047.

References

[1] B. Kienzler, C. Borkel, N. Finck, S. Heck, S. Hilpp, M. Schlieker, V. Metz, M. Plaschke, E. Soballa, T. Cron, A. Miassoedov: Characterization and radionuclide retention properties of heat-treated concrete, Phys. Chem. Earth, 2014, Parts A/B/C Vol. 70–71, 45-52. 10.1016/j.pce.2014.02.004
[2] S. Ma, W. Li, S. Zhang, D. Ge, J. Yu, X. Shen, Influence of sodium gluconate on the performance and hydration of Portland cement, Constr. Build. Mater. 91 (2015) 138–144, https://doi.org/10.1016/j.conbuildmat.2015.05.068.
[3] X. Zhang, Y. He, C. Lu, Z. Huang, Effects of sodium gluconate on early hydration and mortar performance of Portland cement-calcium aluminate cement-anhydrite binder, Constr. Build. Mater. 157 (2017) 1065–1073, https://doi.org/10.1016/j.conbuildmat.2017.09.153.
[4] E. Wieland, L. R. Van Loon: Cementitious Near-Field Sorption Data Base for Performance Assessment of an ILW Repository in Opalinus Clay; PSI Bericht 03-06, 2003, Paul Scherrer Institut
[5] T. Taga, Y. Kuroda, M. Ohashi, Structures of Lanthanoid Complexes of Glyceric Acid, Gluconic Acid, and Lactobionic Acid from the Lanthanoid-Induced ^1H NMR Shifts: pH Dependence of the Lanthanoid-Substrate Equilibria, Bull. Chem. Soc. Jpn. 51 (8) (1978) 2278–2282, https://doi.org/10.1246/bcsj.51.2278.
[6] Z. Zhang, B. Bottenus, S. B. Clark, G. Tian, PL. Zanonato, L. Rao: Complexation of gluconic acid with Nd(III) in acidic solutions: A thermodynamic study, Journal of Alloys and Compounds 444–445 (2007) 470–476. 10.1016/j.jallcom.2007.01.034
[7] S. Giroux, S. Aury, B. Henry, P. Rubini, Complexation of Lanthanide(III) Ions with Polyhydroxy Carboxylic Acids in Aqueous Solutions, Eur. J. Inorg. Chem. (2002) 1162–1168, https://doi.org/10.1002/1099-0682(200205)2002:5<1162::AID-EJIC1162>3.0.CO;2-O.
[8] S. Giroux, P. Rubini, B. Henry, S. Aury, Complexes of praseodymium(III) with D-gluconic acid, Polyhedron 19 (2000) 1567–1574, https://doi.org/10.1016/S0277-5387(00)00422-8.
[9] J. Tits, E. Wieland, M.H. Bradbury, The effect of isosaccharinic acid and gluconic acid on the retention of Eu(III), Am(III) and Th(IV) by calcite, Appl. Geochemistry 20 (2005) 2082–2096, https://doi.org/10.1016/j.apgeochem.2005.07.004.
[10] J.I. Kim, B. Grambow, Geochemical assessement of actinide isolation in a German salt repository environment, Eng. Geol. 52 (1999) 221–230, https://doi.org/10.1016/S0013-7952(99)00007-1.
[11] J.A. Schramke, E.F.U. Santillan, R.T. Peake, Plutonium oxidation states in the Waste Isolation Pilot Plant repository, Appl. Geochemistry 116 (2020), https://doi.org/10.1016/j.apgeochem.2020.104561 104561.
[12] K. Maher, J.R. Bargar, G.E. Brown Jr., Environmental Speciation of Actinides, Inorg. Chem. 52 (2013) 3510–3532, https://doi.org/10.1021/ic301686d.
[13] A.P. Novikov, I.E. Vlasova, A.V. Safonov, V.M. Ermolaev, E.V. Zakharova, S.N. Kalmykov, Speciation of actinides in groundwater samples collected near deep nuclear waste repositories, J. Environ. Radioact. 192 (2018) 334–341, https://doi.org/10.1016/j.jenvrad.2018.07.007.
[14] I.I. Diakonov, B.R. Tagirov, K.V. Ragnarsdottir, Standard Thermodynamic Properties and Heat Capacity Equations for Rare Earth Element Hydroxides Radiochim, Acta. 81 (1998) 107–116, https://doi.org/10.1016/S0009-2541(98)00088-6.
[15] P.J. Panak, A. Geist, Complexation and Extraction of Trivalent Actinides and Lanthanides by Triazinylpyridine N-Donor Ligands, Chem. Rev. 113 (2013) 1199–1236, https://doi.org/10.1021/cr3003399.

[16] V. Neck, M. Altmaier, T. Rabung, J. Lützenkirchen, T. Fanghänel: Thermodynamics of trivalent actinides and neodymium in NaCl, MgCl2, and CaCl2 solutions: Solubility, hydrolysis, and ternary Ca–M(III)–OH complexes, Pure Appl. Chem., 2009, Vol. 81, No. 9, 1555–1568. https://doi.org /10.1351/PAC-CON-08-09-05
[17] G.R. Choppin, E.N. Rizkalla, Lanthanides/Actinides: Chemistry, Handbook on Physics and Chemistry of Rare Earths (1994) 559–590, https://doi.org/10.1016/S0168-1273(05)80051-0.
[18] Y.-M. Chen, C.-Z. Wang, Q.-Y. Wu, J.-H. Lan, ZhiFang Chai, Chang-Ming Nie, Wei-Qun Shi: Complexation of trivalent lanthanides and actinides with diethylenetriaminepentaacetic acid: Theoretical unraveling of bond covalency, J. Mol. Liq. 299 (2020), https://doi.org/10.1016/j.molliq.2019.112174 112174.
[19] Z.-M. Wang, L.J. van de Burgt, G.R. Choppin, Spectroscopic study of lanthanide (III) complexes with aliphatic dicarboxylic acids, Inorganica Chim. Acta. 310 (2000) 248–256, https://doi.org/10.1016/S0020-1693(00)00259-0.
[20] P.L. Zanonato, P. Di Bernardo, A. Bismondo, L. Rao, G.R. Choppin, Thermodynamic Studies of the Complexation between Neodymium and Acetate at Elevated Temperatures, J. Solution Chem. Vol. 30, No. 1 (2001), https://doi.org/10.1023/A:1005227108686.
[21] A. Mondry, P. Starynowicz, Ten-Coordinate Neodymium(III) Complexes with Triethylenetetraaminehexaacetic Acid, Eur. J. Inorg. Chem. (2006) 1859–1867, https://doi.org/10.1002/ejic.200501023.
[22] T.G. Levitskaia, Y. Chen, J.L. Fulton, S.I. Sinkov, Neodymium(III) complexation by amino-carbohydrates *via* a ligand-controlled hydrolysis mechanism, Chem. Commun. 47 (2011) 8160–8162, https://doi.org/10.1039/c1cc11871d.
[23] L. Rao, D. Rai, A.R. Felmy, Solubility of $Nd(OH)_3(c)$ in 0.1 M NaCl Aqueous Solution at 25 °C and 90 °C, Radiochim. Acta. 72 (1996) 151–155, https://doi.org/10.1524/ract.1996.72.3.151.
[24] E. Bentouhami, G.M. Bouet, J. Meullemeestre, F. Vierling, M.A. Khan, Physicochemical study of the hydrolysis of Rare-Earth elements (III) and thorium (IV), C. R. Chimie 7 (2004) 537–545, https://doi.org/10.1016/j.crci.2004.01.008.
[25] Y.F. Orlov, E.I. Maslov, E.I. Belkina, Solubilities of Metal Hydroxides, Russ. J. Inorg. Chem. 58 (11) (2013) 1306–1314, https://doi.org/10.1134/S0036023613110168.
[26] B. Kutus, N. Varga, G. Peintler, A. Lupan, A.A.A. Attia, I. Pálinkó, P. Sipos, Formation of mono- and binuclear neodymium(III)– gluconate complexes in aqueous solutions in the pH range of 2–8, Dalton Trans. 46 (2017) 6049–6058, https://doi.org/10.1039/c7dt00909g.
[27] É. Böszörményi, J. Lado, C.s. Jorge, B. Dudás, M. Kutus, G. Szabados, I. Varga, P.S. Palinkó, The structure and composition of solid complexes comprising of Nd (III), Ca(II) and D-gluconate isolated from solutions relevant to radioactive waste disposal, Pure and Appl. Chem. 92 (2020) 10, https://doi.org/10.1515/pac-2019-1010.
[28] P. Warwick, N. Evans, T. Hall, S. Vines, Stability constants of uranium(IV)-alpha-isosaccharinic acid and gluconic acid complexes, Radiochim. Acta. 92 (2004) 897–902, https://doi.org/10.1524/ract.92.12.897.55106.
[29] L. Ciavatta, R. Porto, E. Vasca, Hydrolysis of the neodymium(III) ion, Nd3+, in 3 m (Li)ClO_4 medium at 60 °C, Polyhedron 8 (22) (1989) 2701–2707, https://doi.org/10.1016/S0277-5387(00)80442-8.
[30] G. Peintler, B. Kormányos, B. Gyurcsik: pHCali, A Program for Accurate Calibration of pH-metric Instruments, Versions 1.00–1.32, Department of Physical Chemistry, University of Szeged, Hungary (2007–2012)
[31] L. Zékány, I. Nagypál and G. Peintler, Manual for PSEQUAD, Update 5.20, Hungary, 2018.
[32] Á. Buckó, B. Kutus, G. Peintler, I. Pálinkó, P. Sipos, Temperature dependence of the acid–base and Ca^{2+}-complexation equilibria of D-gluconate in hyperalkaline aqueous solutions, Polyhedron 158 (2019) 117–124, https://doi.org/10.1016/j.poly.2018.10.034.
[33] Z. Zhang, P. Gibson, S.B. Clark, G. Tian, P.L. Zanonato, L. Rao, Lactonization and Protonation of Gluconic Acid: A Thermodynamic and Kinetic Study by Potentiometry, NMR and ESI-MS, J. Solution Chem. 36 (2007) 1187–1200, https://doi.org/10.1007/s10953-007-9182-x.
[34] B. Kutus, G. Peintler, Á. Buckó, Zs. Balla, A. Lupan, A. A. A. Attiac, I. Pálinkó, P. Sipos: The acidity and self-catalyzed lactonization of L-gulonic acid: Thermodynamic, kinetic and computational study, Carbohydrate Research 467 (2018) 14–22. 10.1016/j.carres.2018.07.006
[35] G. Peintler, I. Nagypál, A. Jancsó, I.R. Epstein, K. Kustin, Extracting Experimental Information from Large Matrixes. 1. A New Algorithm for the Application of Matrix Rank Analysis, Journal of Physical Chemistry A 101 (1997) 8013–8020.
[36] D.F. Mullica, G.A. Wilson, C.K.C. Lok, An Investigation of the Hypersensitive Pseudo-quadrupole Transitions of Neodymium(III) Complexes and their Induced NMR Chemical Shifts, Inorg. Chim. Acta 156 (1989) 159–161, https://doi.org/10.1016/S0020-1693(00)83490-8.
[37] W.R. Carper, D.B. Coffin, NMR Studies of Paramagnetic Metal Ion Interactions with Gluconate and 1,5-Gluconolactone, Inorg. Chim. Acta 167 (1990) 261–264, https://doi.org/10.1016/S0020-1693(00)80507-1.
[38] M.M. Akhmetov, G.G. Gumarov, V.Yu. Petukhov, M.Yu. Volkov, NMR study of sodium gluconate solutions, J. Mol. Struct. 1193 (2019) 373–377, https://doi.org/10.1016/j.molstruc.2019.05.061.
[39] A. Pallagi, P. Sebők, P. Forgó, T. Jakusch, I. Pálinkó, Pál Sipos: Multinuclear NMR and molecular modelling investigations on the structure and equilibria of complexes that form in aqueous solutions of Ca^{2+} and gluconate, Carbohydr. Res. 345 (2010) 1856–1864, https://doi.org/10.1016/j.carres.2010.05.009.
[40] A. González Fá, I. López-Corral, R. Faccio, A. Juan, M.S. Di Nezio: Surface enhancement Raman spectroscopy and density functional theory study of silver nanoparticles synthetized with d-glucose, J. Raman Spectrosc. 49 (2018) 1756, 10.1002/jrs.5466.
[41] M. Kačuráková, M. Mathlouthi, FTIR and laser-Raman spectra of oligosaccharides in water: characterization of the glycosidic bond, Carbohydr. Res. 284 (1996) 145, https://doi.org/10.1016/0008-6215(95)00412-2.
[42] P.D. Vasko, J. Blackwell, J.L. Koenig: Infrared and raman spectroscopy of carbohydrates.: Part II: Normal coordinate analysis of α-D-glucose, Carbohydr. Res. 23 (1972) 407, 10.1016/S0008-6215(00)82690-7.
[43] N.J. Hess, Y. Xia, A.R. Felmy, Nuclear Waste Management, American Chemical Society (2006) 286–301.
[44] S.K. Papageorgiou, E.P. Kouvelos, E.P. Favvas, A.A. Sapalidis, G.E. Romanos, F.K. Katsaros, Metal-carboxylate interactions in metal-alginate complexes studied with FTIR spectroscopy, Carbohydr. Res. 345 (2010) 469, https://doi.org/10.1016/j.carres.2009.12.010.
[45] V. Zelenak, Z. Vargova, K. Gyoryova, Correlation of infrared spectra of zinc(II) carboxylates with their structures, Spectrochim. Acta A. Mol. Biomol. Spectrosc. 66 (2007) 262, https://doi.org/10.1016/j.saa.2006.02.050.
[46] J.N. van Niekerk, F.R.L. Schoening, X-Ray Evidence for Metal-to-Metal Bonds in Cupric and Chromous Acetate, Nature 171 (1953) 36, https://doi.org/10.1038/171036a0.